5264 *Chem. Mater.* **2009,** *21,* 5264–5271
DOI:10.1021/cm902322e

CHEMISTRY OF MATERIALS
Article

General Layer-By-Layer Approach To Composite Nanotubes and Their Enhanced Lithium-Storage and Gas-Sensing Properties

Ning Du, Hui Zhang,* Jingxue Yu, Ping Wu, Chuanxin Zhai, Yanfang Xu, Jiazheng Wang, and Deren Yang

State Key Lab of Silicon Materials and Department of Materials Science and Engineering, Zhejiang University, Hangzhou 310027, People's Republic of China

Received July 29, 2009. Revised Manuscript Received September 28, 2009

A novel and versatile layer-by-layer approach has been developed to synthesize composite metal oxide nanotubes on carbon-nanotube (CNT) templates. We demonstrate this approach by the preparation of CeO_2-SnO_2 and Ag−NiO composite nanotubes. The electrostatic attraction between the CNTs and metal ions play the most important role in the formation of CNT-based core−shell nanotubes, from which the composite metal oxide nanotubes are subsequently synthesized. It is found that the CeO_2-SnO_2 and Ag−NiO composite nanotubes lead to excellent device performance when they are used in gas sensors and Li-ion batteries, respectively.

Introduction

Nanotubes have emerged as a fascinating class of nanomaterials because of their superior performance in numerous applications such as energy storage, gas sensing, drug delivery, and electronic and optoelectronic devices.[1−10] All these applications critically depend on the controlled syntheses of nanotubes. Up to now, many approaches have been developed to synthesize nanotubes. They are usually either template-free[11,12] or template-assisted methods.[13,14] Given the complexity of fabrication, the range of application, and the control of size and shape, template-assisted approaches are more advantageous than template-free ones.[14] In all kinds of template-assisted approaches, anodic aluminum oxide (AAO) templates are the most widely used owing to the tunable pore dimensions, good mechanical strength, and structural stability. Nevertheless, there are a few disadvantages of the use of AAO templates to synthesize nanotubes. First, large-scale synthesis is impractical. This hinders the wide application of the AAO-assisted approach. Second, it is very difficult to completely remove the AAO templates. Third, the diameters of as-synthesized metal oxide nanotubes are usually larger than 100 nm. To avoid the AAO-template related disadvantages, as-received one-dimensional nanostructure such as nanorods, nanowires, and nanotubes have been used as alternative templates to synthesize nanotubes.[15−18] As one of the most typical one-dimensional nanomaterials, carbon nanotubes (CNTs) have been considered to be the ideal templates for the synthesis of metal oxide nanotubes due to their mass production, chemical stability, and facial modification.[19−23] It is widely accepted that homogeneous and dense deposition of metal oxide layers on the surface of CNTs is a prerequisite for the preparation of metal oxide nanotubes. For example, Rao and his co-workers developed a metal-alkoxide-based sol−gel process to densely deposit metal oxide layers on the surface of CNTs. ZrO_2, Al_2O_3, V_2O_5, SiO_2, and MoO_3 nanotubes were subsequently obtained after calcination.[19−21] Liu and his co-workers reported the synthesis of CNT-Fe_2O_3

*Author to whom correspondence should be addressed. E-mail: msezhanghui@zju.edu.cn. Tel.: +86 571 87951667. Fax: +86 571 87952322.

(1) Macak, J. M.; Tsuchiya, H.; Ghicov, A.; Schmuki, P. *Electrochem. Commun.* **2005**, *7*, 1133.
(2) Mor, G. K.; Shankar, K.; Paulose, M.; Varghese, O. K.; Grimes, C. A. *Nano Lett.* **2006**, *6*, 215.
(3) Chen, J.; Tao, Z. L.; Li, S. L. *Angew. Chem., Int. Ed.* **2003**, *42*, 2147.
(4) Wang, Y.; Lee, J. Y.; Zeng, H. C. *Chem. Mater.* **2005**, *17*, 3889.
(5) Yu, S. F.; Welp, U.; Hua, L. Z.; Rydh, A.; Kwok, W. K.; Wang, H. H. *Chem. Mater.* **2005**, *17*, 3445.
(6) Varghese, O. K.; Gong, D.; Paulose, M.; Ong, K. G.; Grimes, C. A. *Sens. Actuators B* **2003**, *93*, 338.
(7) Son, S. J.; Reichel, J.; He, B.; Schuchman, M.; Lee, S. B. *J. Am. Chem. Soc.* **2005**, *127*, 7316–7317.
(8) Chen, C. C.; Liu, Y. C.; Wu, C. H.; Yeh, C. C.; Su, M. T.; Wu, Y. C. *Adv. Mater.* **2005**, *17*, 404–407.
(9) Ebbesen, T. W.; Lezec, H. J.; Hiura, H.; Bennett, J. W.; Ghaemi, H. F.; Thio, T. *Nature* **1996**, *382*, 54.
(10) Ajayan, P. M. *Chem. Rev.* **1999**, *9*, 1787.
(11) Remskar, M. *Adv. Mater.* **2004**, *16*, 1497.
(12) Tenne, R. *Nat. Nanotechnol.* **2006**, *1*, 103.
(13) Martin, C. R. *Science* **1994**, *266*, 1961.
(14) Bae, C.; Yoo, H.; Kim, S.; Lee, K.; Kim, J.; M. Sung, M.; Shin, H. *Chem. Mater.* **2008**, *20*, 756.
(15) Hwang, J.; Min, B.; Lee, J. S.; Keem, K.; Cho, K.; Sung, M.; Lee, M.; Kim, S. *Adv. Mater.* **2004**, *16*, 422.
(16) Peng, Q.; Sun, X. Y.; Spangnola, J. C.; Hyde, G. K.; Spontak, R. J.; Parsons, G. N. *Nano Lett.* **2007**, *7*, 719.
(17) Mayya, K. S.; Gittins, D. I.; Dibaj, A. M.; Caruso, F. *Nano Lett.* **2001**, *1*, 727.
(18) Liu, Z. Q.; Zhang, D. H.; Han, S.; Li, C.; Lei, B.; Lu, W. G.; Fang, J. Y.; Zhou, C. W. *J. Am. Chem. Soc.* **2005**, *16*, 6.
(19) Rao, C. N. R.; Satishkumar, B. C.; Govindaraj, A. *Chem. Commun.* **1997**, 1581.
(20) Ogihara, H.; Sadakane, M.; Nodasaka, Y.; Ueda, W. *Chem. Mater.* **2006**, *18*, 4981.
(21) Satishkumar, B. C.; Govindaraj, A.; Nath, M.; Rao, C. N. R. *J. Mater. Chem.* **2000**, *10*, 2115.
(22) Sun, Z. Y.; Yuan, H. Q.; Liu, Z. M.; Han, B. X.; Zhang, X. R. *Adv. Mater.* **2005**, *17*, 2993.
(23) Zhang, Y. J.; Liu, J.; He, R. R.; Zhang, Q.; Zhang, X.; Zhu, J. *Chem. Phys. Lett.* **2002**, *356*, 579.

 Published on Web 10/15/2009

core−shell nanotubes and polycrystalline Fe_2O_3 nanotubes by a supercritical-fluid route and subsequent calcination.[22] Moreover, coating a metal oxide layer on CNTs was also achieved by a chemical vapor deposition process.[23] More recently, we have reported the layer-by-layer (LBL) and metal carbonyl decomposition methods for the synthesis of metal oxide nanotubes using CNT templates.[24,25] The as-synthesized metal oxide nanotubes were applied in gas sensors and lithium-ion batteries, which showed the improved performance in comparison with the corresponding nanoparticles and bulk materials. Much more efforts should be employed to further enhance their comprehensive properties for practical application by doping or compositing another component. However, the synthesis of composite metal oxide nanotubes on CNT templates remains tremendous challenge because it is very difficult to deposit uniform and dense composite metal oxide layers on the surface of CNTs.

In this work, we propose a novel and versatile approach to synthesize composite metal oxide nanotubes by LBL assembly and subsequent calcination on CNT templates for the first time. CeO_2−SnO_2 and Ag−NiO composite nanotubes have been prepared by this approach. Moreover, the as-synthesized CeO_2−SnO_2 and Ag−NiO composite nanotubes are applied in gas sensors and Li-ion batteries, respectively.

Experimental Section

Synthesis of CeO_2−SnO_2 Nanotubes. The carbon nanotubes (CNTs) with diameters of about 30−50 nm were purchased from Times-nano Nanotech Co. Ltd. and used without further purification. Poly(diallyldimethylammonium chloride) (PDDA), M_w < 500 000 Da, and poly(sodium 4-styrenesulfonate) (PSS), M_w < 70 000 Da, were purchased from Alfa Aesar Co. Ltd. The CNTs were first modified by polyelectrolyte (PDDA/PSS). Briefly, 30 mg CNTs were sonicated for 1 h in 50 mL 1 M NaCl solution, and 80 mg PDDA was added and stirred for 0.5 h. Subsequently, the excess PDDA was removed by six repeated centrifugation/wash cycles. Similarly, the PSS layers were further coated on the surface of the PDDA modified CNTs to obtain the PDDA/PSS modified CNTs. The regular CeO_2−SnO_2 nanotubes were achieved as follows: the PDDA/PSS modified CNTs were put into 100 mL water with 0.04 g $Ce(NO_3)_3$, which was sonicated for 10 min. Then, 20 mL NaOH (0.05 mol/L) aqueous solution was slowly dropped into the above-mentioned solution at room temperature. After 0.5 h, the resulting black solid products were centrifuged, washed with distilled water, and subsequently modified by PDDA by above-mentioned approach. The as-prepared solid products were put into 100 mL water with 0.1 g $NaBH_4$ and stirred for 10 min. Then, 20 mL $SnCl_4$ (9 g/L) solution was dropped into the above-mentioned solution at room temperature. After 0.5 h, the resulting black solid products were centrifuged, washed with distilled water. Finally, the black products were annealed at 550 °C in O_2 for 3 h to remove the CNTs, and the white solid products were obtained. CeO_2−SnO_2 nanoparticles were synthesized by the same approach without the assistance of CNT templates.

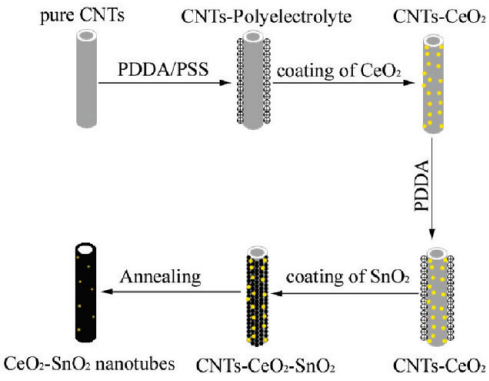

Figure 1. Schematic illustration for the LBL synthesis of CeO_2−SnO_2 nanotubes.

Synthesis of Ag−NiO Nanotubes. The CNTs were first modified by polyelectrolyte (PDDA/PSS) in sequence through the above-mentioned process. The PDDA/PSS modified CNTs were put into 100 mL solution with 0.1 mmol $AgNO_3$ and 0.2 g PVP (polyvinylpyrrolidone). Then, 40 mL 0.05 M $NaBH_4$ solution was dropped into the above-mentioned solution. After 0.5 h, the resulting black solid products were centrifuged, washed with distilled water, and subsequently modified by PDDA again by the approach as mentioned above. The as-prepared black products were put into 50 mL water with 0.23 g $NiCl_2$ and 0.42 g citric acid. Then, 40 mL 0.05 M $NaBH_4$ solution was dropped into the above-mentioned solution at room temperature. After 0.5 h, the resulting black solid products were centrifuged and washed with distilled water. Finally, the black products were annealed at 550 °C in O_2 for 3 h to remove the CNTs, and the gray solid products were obtained. The NiO nanotubes were synthesized by the approach in ref 24.

Gas Sensor Characterization of CeO_2−SnO_2 Nanotubes. The CeO_2−SnO_2 nanotube films were fabricated on the top of the Au electrodes (3 cm × 3 cm) by spin coating, followed by annealing at 100 °C for 3 h before electrical and gas sensing measurement. The gas-sensing behavior of the CeO_2−SnO_2 nanotube based sensor was measured at room temperature using the Keithley 4200 source measure unit. The chamber was first purged by N_2 until a steady baseline of the sensor resistance was reached. Then, the tested vapor, C_2H_5OH, was injected at a fixed concentration of 500 ppm in N_2. In general, the DC voltage was fixed at 10 V, and the change of current with the time was recorded. The sensitivity S was defined as I_g/I_a, where I_g and I_a were the current through the sensor in the tested gas after exposing for 10 min and that in air, respectively. The response and recovery time of the sensor was defined as the time needed to reach 90% of the original resistance.

Electrochemical Measurements of Ag−NiO Nanotubes. Electrochemical measurements were carried out using two-electrode cells with lithium metal as the counter and reference electrodes. The working electrodes were composed of the active material (Ag−NiO nanotubes), conductive material (acetylene black, ATB), and binder (polytetrafluoroethylene, PTFE) in a weight ratio of Ag−NiO/ATB/PTFE = 14:3:3. The electrode was dried at 80 °C for 1 h and cut into a piece of disk (1.0 cm^{-2}). The electrolyte solution was 1 M $LiPF_6$ dissolved in a mixture of ethylene carbonate (EC), propylene carbonate (PC), and diethyl carbonate (DEC) with the volume ratio of EC/PC/DEC = 3:1:1. The cell assembly was performed in a glovebox filled with pure argon (99.999%) in the presence of an oxygen scavenger and a

(24) Du, N.; Zhang, H.; Chen, B. D.; Ma, X. Y.; Liu, Z. H.; Wu, J. B.; Yang, D. *Adv. Mater.* **2007**, *19*, 1641.
(25) Du, N.; Zhang, H.; Chen, B. D.; Wu, J. B.; Ma, X. Y.; Liu, Z. H.; Zhang, Y. Q.; Yang, D.; Huang, X. H.; Tu, J. P. *Adv. Mater.* **2007**, *19*, 4505.

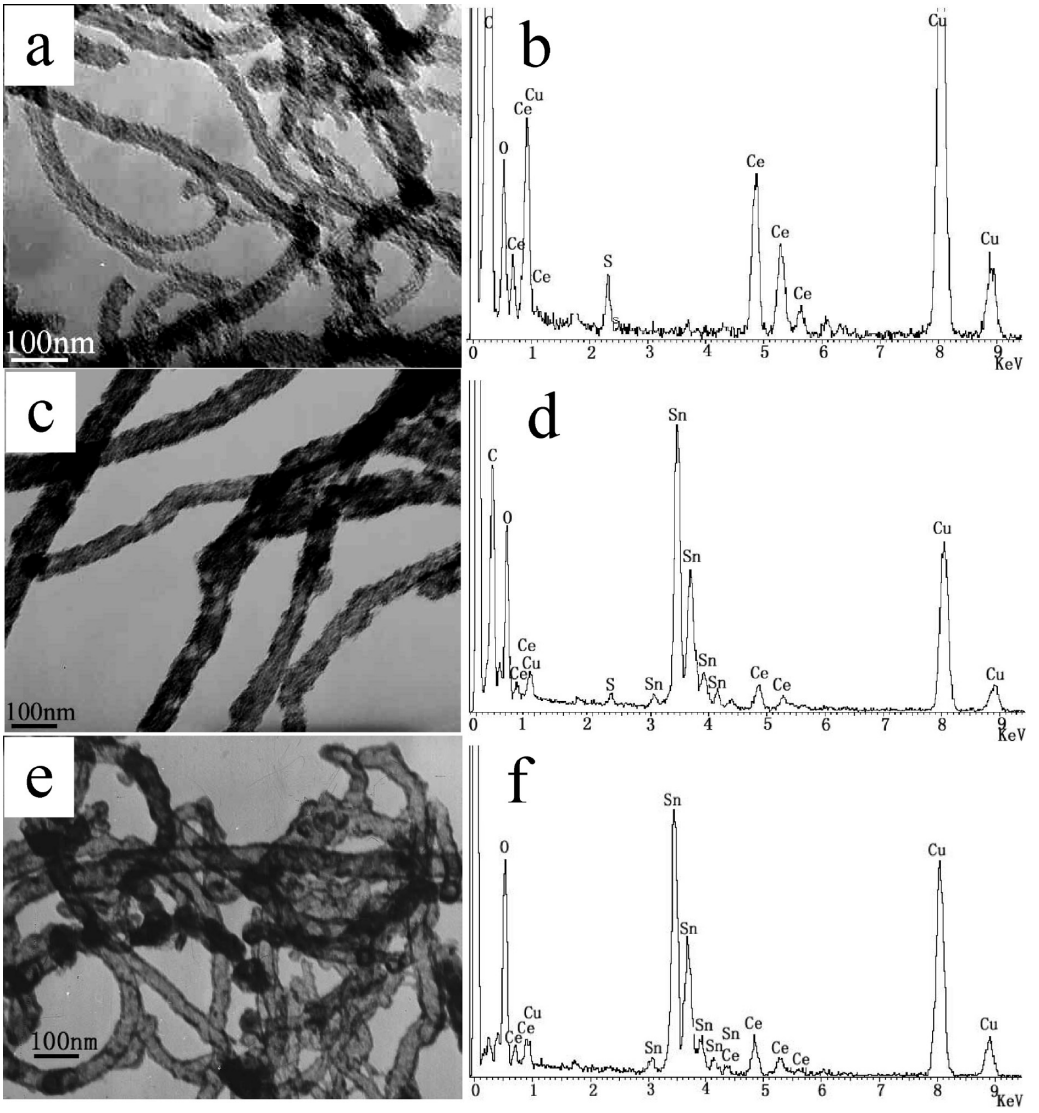

Figure 2. TEM images of CNT-CeO_2 (a), CNT-CeO_2−SnO_2 (c), and CeO_2−SnO_2 (e) nanotubes and the corresponding EDX patterns (b, d, f).

sodium-drying agent. The electrode capacity was measured by a galvanostatic discharge−charge method at a current density of 100 $mA \cdot g^{-1}$ and 20 °C. Charge−discharge cycles were tested with a current density of 100 $mA \cdot g^{-1}$ in the potential range of 0.01−3 V.

Results and Discussion

As schematically illustrated in Figure 1, a layer of polyelectrolyte, e.g. poly(diallyldimethylammonium chloride) (PDDA) and sodium poly(styrenesulfonate) (PSS), was first coated onto the surface of pristine CNTs by LBL assembly, thus enabling the CNTs to be negatively charged. An aqueous solution of $Ce(NO_3)_3$ was then added into the polyelectrolyte-modified CNT solution. The positively charged Ce^{3+} was adsorbed onto the surface of negatively charged CNTs due to the electrostatic attraction between the charged species. Subsequently, the NaOH aqueous solution was gradually dropped into the above-mentioned solution, resulting in the deposition of CeO_2 onto the surface of CNTs. For further deposition of SnO_2 layer, another PDDA layer was coated on the surface of CNT-CeO_2 nanotubes via LBL assembly, enabling the surface of CNT-CeO_2 nanotubes to be positively charged. An aqueous solution of $NaBH_4$ was then added into the PDDA-modified CNT-CeO_2 nanotube solution. The negatively charged BH_4^- was adsorbed onto the positively charged CNT-CeO_2 nanotubes. By gradually dropping $SnCl_4$ solution into the above-mentioned solution, a SnO_2 layer was deposited onto the surface of CNT-CeO_2 nanotubes. Finally, the CeO_2−SnO_2 composite nanotubes were obtained by calcination of CNT-CeO_2−SnO_2 nanotubes.

Figure 2a and b shows the transmission electron microscopy (TEM) image and corresponding energy dispersive X-ray (EDX) pattern of CNT-CeO_2 nanocomposites. A rough CeO_2 layer is deposited onto the surface of CNTs (Figure 2a). We do not observe any nanoparticles in the solution except at the surface of CNTs. This indicates the formation of high-quality CNT-CeO_2 nanocomposites. The electrostatic attraction between negatively charged CNTs and positively charged Ce^{3+} results in the dense deposition of CeO_2 at the surface of CNTs. From the

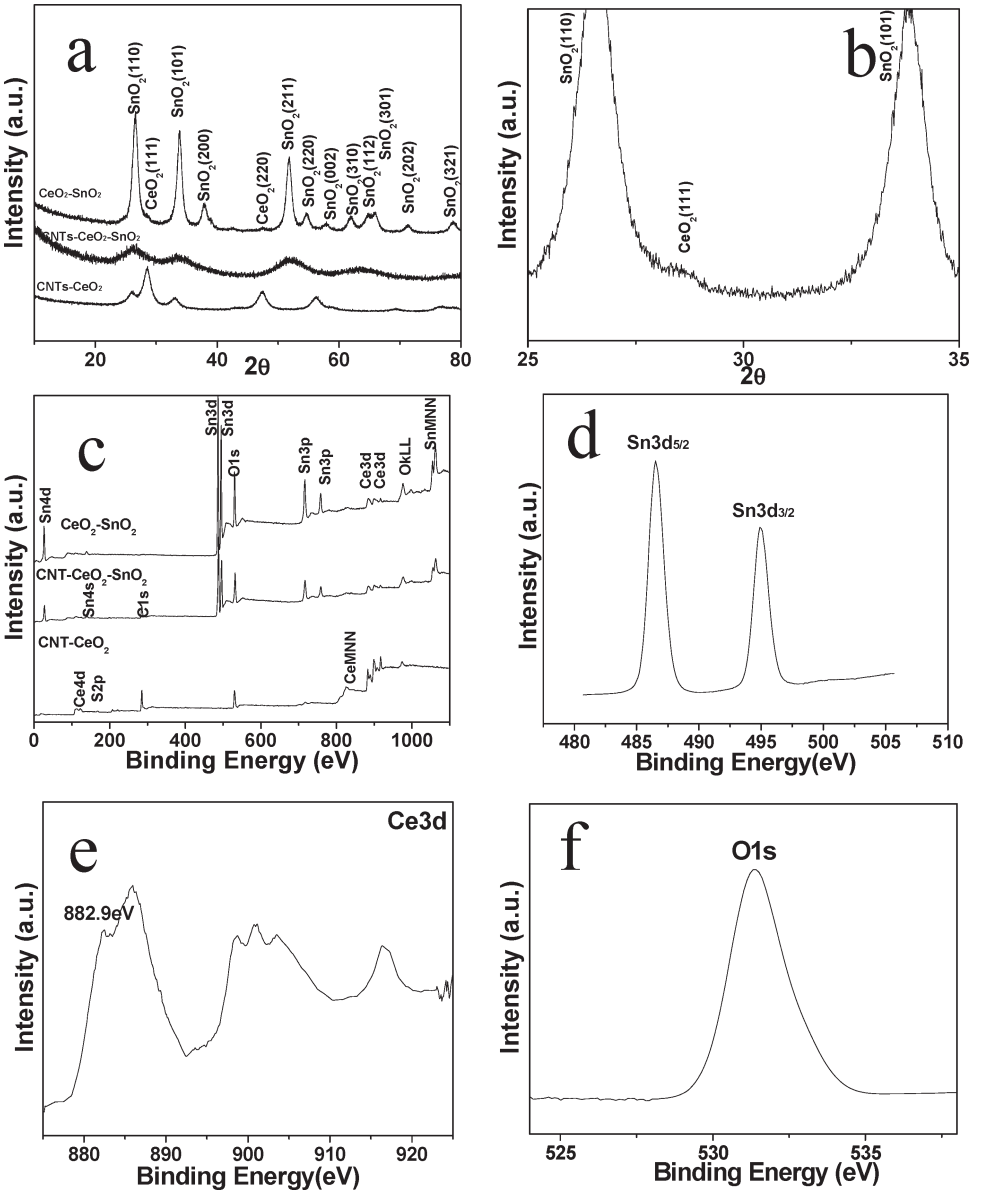

Figure 3. XRD pattern (a, b) and XPS spectra (c−f) evolution along with LBL assembly of CeO_2 and SnO_2 on CNTs template.

EDX pattern, we see the peaks of Cu, C, Ce, O, and S, which originate from TEM grids, CNTs, and the CeO_2 layer and polyelectrolyte, respectively. The EDX analysis further confirms the formation of CNT-CeO_2 nanocomposites. After the coating of SnO_2, a thicker SnO_2 layer is deposited onto the surface of CNT-CeO_2 nanocomposites (Figure 2c). A strong Sn peak emerges in the EDX pattern (Figure 2d), which reveals the formation of CNT-CeO_2−SnO_2 nanocomposites. Moreover, the Ce/Sn molar ratio of CNT-CeO_2−SnO_2 nanocomposites is about 8% according to EDX analysis. Figure 2e shows the TEM image of the product prepared by the calcination of CNT-CeO_2−SnO_2 nanocomposites at 550 °C in oxygen atmosphere. It is observed that CNTs are removed by oxidation and that the tube-like structures are maintained. Figure 2f shows the corresponding EDX pattern. It is clear that the peaks of C and S disappear due to the removal of CNTs and polyelectrolyte. Therefore, the TEM and EDX analysis confirm the formation of CeO_2−SnO_2 nanotubes.

Figure 3a shows the evolution of the X-ray diffraction (XRD) pattern along with the LBL assembly of CeO_2 and SnO_2 on CNT templates. All the peaks can be assigned to cubic CeO_2 and CNTs after deposition of CeO_2 on CNT templates, indicating the formation of CNT-CeO_2. After the coating of SnO_2, the peaks of tetragonal SnO_2 emerge beside the peaks of CNTs and CeO_2. This demonstrates the formation of CNT-CeO_2−SnO_2. After calcination, the peaks of CNTs disappear, while those of CeO_2 and SnO_2 become stronger. The existence of the peak of CeO_2 can be further verified by magnified XRD pattern (Figure 3b). This is caused by the removal of CNTs and crystallization of CeO_2 and SnO_2. Moreover, the broadened XRD diffraction peaks indicate that the coating layers are composed of CeO_2 and SnO_2 nanoparticles. Figure 3c shows XPS spectra collected in the preparation of CeO_2−SnO_2 nanotubes. The elements carbon (C), cerium (Ce), oxygen (O), and sulfur (S) are detected from the CNT-CeO_2 nanocomposites. C originates from

CNTs. Ce and O is from CeO_2. S is introduced by the polyelectrolyte. Sn peaks appear after the LBL assembly of SnO_2. After calcination, C and S peaks disappear due to the removal of CNTs and the polyelectrolyte. Figure 3d−f shows the multiplex spectra of Sn, Ce, and O. The peaks of tin at 487.6 and 496.0 eV can be assigned to Sn $3d_{5/2}$ and $3d_{3/2}$ of the tetravalent state, respectively (Figure 3d).[26] Figure 3e shows the multiplex spectrum of Ce peaks. The peak with binding energies of 882.9 eV corresponds to Ce 3d of the tetravalent state.[27] No other valence state of Sn and Ce can be found which further identify the formation of CeO_2−SnO_2 nanotubes. Scanning electron microscopy (SEM), high-resolution TEM (HRTEM), and element mapping analysis were used to further characterize CeO_2−SnO_2 nanotubes. Figure 4a shows the SEM image of CeO_2−SnO_2 nanotubes. It can be seen that the as-synthesize products maintain the structure of CNTs. The opening nanotubular structure can be verified by the magnified SEM image (Figure 4b). Figure 4c shows the TEM image of CeO_2−SnO_2 nanotubes. The tubelike morphology is observed with the wall thickness of about 5 nm. The HRTEM image (Figure 4d) shows that the nanotube is composed of nanoparticles with a diameter of about 3 nm. There are two lattice fringes with lattice spacings of 0.31 and 0.34 nm corresponding to the CeO_2 {111} and SnO_2 {110} planes from different grains, respectively. We believe that CeO_2−SnO_2 nanotubes are polycrystalline in nature. Figures 4e and f show the EDX mapping images of Sn and Ce. It is clear that these two elements are evenly distributed in the nanotubes. The density of Sn is much larger than that of Ce.

It is known that SnO_2 has been considered as the most promising of gas-sensing materials, due to its superior gas-sensing performance. However, SnO_2 can respond to almost all reducing gas, resulting in decreased selectivity.[28] At present, doping or combining of another component is used to enhance the selectivity.[29,30] In addition, thin films SnO_2 or bulk SnO_2 need a high working temperature due to their low surface-to-volume ratio. The use of porous SnO_2 or nano-SnO_2 materials may solve this problem somewhat.[31,32] Recently, Khodadadi and his co-workers reported that the CeO_2-doped SnO_2 thin films exhibited enhanced sensitivity and selectivity to ethanol.[33] We therefore expected that CeO_2−SnO_2 nanotubes may exhibit superior ethanol-sensing performance, resulting from the combining of CeO_2 and large surface-to-volume ratios. Figure 5a shows the sensitivity response of CeO_2−SnO_2 nanotube-based gas sensors versus the

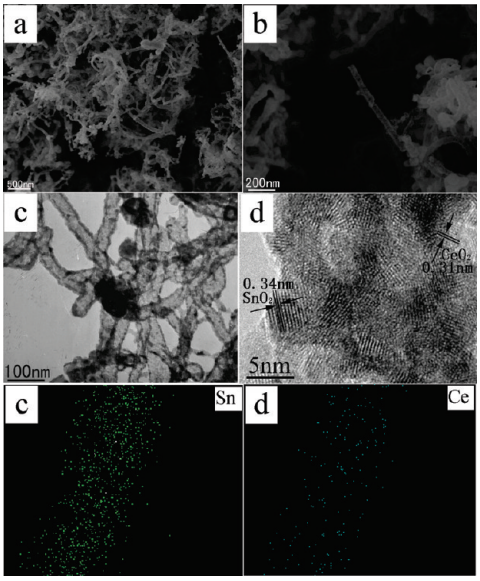

Figure 4. Morphological and structural characterization of CeO_2−SnO_2 nanotubes: (a, b) SEM image; (c) TEM image; (d) HRTEM image; (e, f) EDX mapping images of Sn and Ce.

time for 500 ppm ethanol at room temperature. It is seen that CeO_2−SnO_2 nanotubes respond well to ethanol with a high sensitivity of 65. The response time and recovery time are short (less than 50 s). The reproducibility is rather good with relatively minor deviations for six replicates. Figure 5b shows sensitivity response versus ethanol concentration (100−1000 ppm) at room temperature for the gas sensors based on CeO_2−SnO_2 nanotubes and those based on CeO_2−SnO_2 nanoparticles. As observed, the sensitivity of the two types of gas sensors increase rapidly with ethanol concentration. The gas sensors based on CeO_2−SnO_2 nanotubes are more sensitive than those based on CeO_2−SnO_2 nanoparticles. In order to study the selectivity, the CeO_2−SnO_2 nanotubes and SnO_2 nanotubes were applied in four types of gas sensors such as CO, CH_4, C_2H_5OH, and NH_3 with the same concentration of 500 ppm (Figure 5c). We see that CeO_2−SnO_2 nanotubes are more sensitive to ethonal than other three types of gases. In contrast, there is little difference in sensitivity to CO, CH_4, C_2H_5OH, and NH_3 for the gas sensor based on SnO_2 nanotubes. Therefore, the gas sensor based on CeO_2−SnO_2 nanotubes shows better selectivity to ethanol than that based on SnO_2 nanotubes. The large surface-to-volume ratio, polycrystallinity, nanotubular structure, and the combining of CeO_2 may be responsible for the improved sensing of ethanol.

In order to confirm the universality of this method for synthesizing composite metal oxide nanotubes, Ag−NiO nanotubes have been fabricated by this approach. Figure 6a and b shows the field emission SEM (FESEM) image and magnified FESEM image of Ag−NiO nanotubes. It can be seen that these nanotubes are 30−50 nm in diameter and several micrometers in length, which is evidenced by the TEM image (Figure 6c). No nanoparticles are observed in the solution, indicating the formation of high-quality Ag−NiO nanotubes.

(26) Ahn, H. J.; Choi, H. C.; Park, K. W.; Kim, S. B.; Sun, Y. E. *J. Phys. Chem. B.* **2004**, *108*, 9815.
(27) Ho, C.; Yu, J. C.; Kwong, T.; Mak, A. C.; Lai, S. *Chem. Mater.* **2005**, *17*, 4514.
(28) Sberveglieri, G. *Sens. Actuators B* **1995**, *23*, 103.
(29) Behr, G.; Fliegel, W. *Sens. Actuators B* **1995**, *26*, 33.
(30) Salehi, A.; Gholizade, M. *Sens. Actuators B* **2003**, *89*, 173.
(31) Law, M.; Kind, H.; Kim, F.; Messer, B.; Yang, P. *Angew. Chem., Int. Ed.* **2002**, *41*, 2405.
(32) Huang, J.; Matsunaga, M.; Shimanoe, K.; Yamazoe, N.; Kunitake, T. *Chem. Mater.* **2005**, *17*, 3513.
(33) Pourfayaz, F.; Khodadadi, A.; Mortazavi, Y.; Mohajerzadeh, S. S. *Sens. Actuators B* **2005**, *108*, 172.

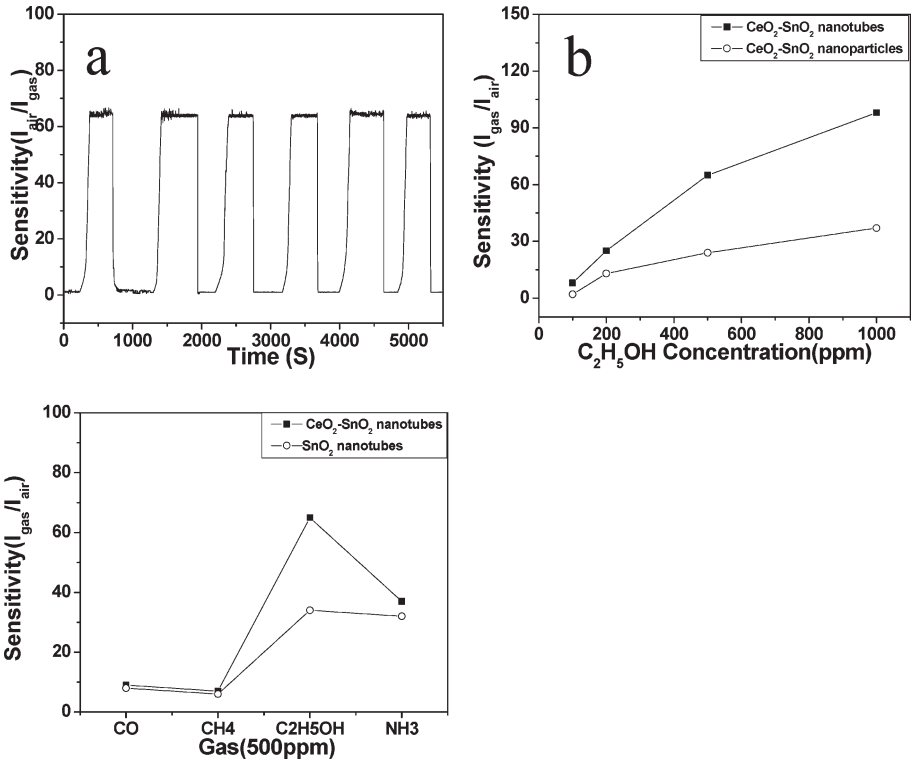

Figure 5. (a) Sensitivity response of the CeO_2-SnO_2 nanotube-based gas sensor versus time for 500 ppm C_2H_5OH at room temperature. (b) Sensitivity response versus C_2H_5OH concentration (100−1000 ppm) at room temperature for two types of gas sensors based on CeO_2-SnO_2 nanotubes and CeO_2-SnO_2 nanoparticles. (c) Sensitivity response versus 500 ppm for four types of gases at room temperature for two types of gas sensors based on CeO_2-SnO_2 nanotubes and SnO_2 nanotubes.

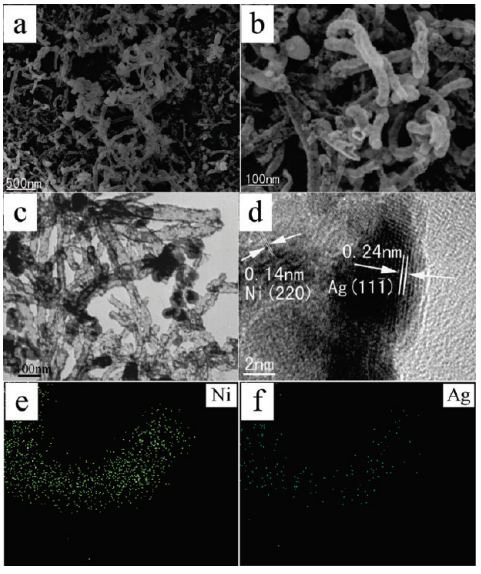

Figure 6. Morphological and structural characterization of Ag−NiO nanotubes: (a, b) SEM image; (c) TEM image; (d) HRTEM image; (e, f) EDX mappings images of Ni and Ag.

Figure 6d shows the HRTEM image of an individual Ag−NiO nanotube. It can be seen that there are two lattice fringes with lattice spacings of 0.24 and 0.14 nm corresponding to the Ag {111} and NiO {220} planes from different grains, respectively. We believe that the Ag−NiO nanotubes are polycrystalline in nature. Figure 6e and f show the EDX mapping images of Ni and Ag. It is clear that these two elements are evenly distributed in the nanotubes. The density of Ni is much larger than that of Ag. Figure 7a and b shows the XRD pattern and magnified XRD pattern of Ag−NiO nanotubes. As can be seen, all diffraction peaks can be assigned to Ag and NiO. This further indicates the formation of Ag−NiO nanotubes. From the EDX pattern (Figure 7c), we see the peaks of Al, Ag, Ni, and O, which originate from the support and Ag−NiO nanotubes, respectively. Figure 7d shows the XPS spectrum of Ag−NiO nanotubes. Nickel (Ni), silver (Ag) and oxygen (O) are detected, which originate from Ag−NiO nanotubes. Figure 7e and f show the multiplex spectra of Ni and Ag. It can be seen that element Ag exists as metal silver and element Ni exists as bivalent oxidation state in the Ag−NiO nanotubes.

Since the discovery of 3d transition metal oxides with good performance as the rechargeable negative-electrode of Li-ion batteries by Tarason and his co-workers, a worldwide effort has been made to improve their energy density, cycle performance, initial, and coulomb efficiency.[34] Among the 3d transition metal oxide, NiO attracts more interest due to its cheaper source than others. In recent years, it is found that hollow nanostructures can improve the Li-ion battery performance.[35−37] More recently, the Ag-NiO films have been proven to

(34) Poizot, P.; Laruelle, S.; Grugeon, S.; Dupont, L.; Tarascon, J. M. *Nature* **2000**, *407*, 496.
(35) Cao, A. M.; Hu, J. S.; Liang, H. P.; Wan, L. J. *Angew. Chem., Int. Ed.* **2005**, *44*, 4391.
(36) Li, W. Y.; Xu, L. N.; Chen, J. *Adv. Funct. Mater.* **2005**, *15*, 851.
(37) Cai, F. S.; Zhang, G. Y.; Chen, J.; Gou, X. L; Liu, H. K.; Dou, S. X. *Angew. Chem., Int. Ed.* **2004**, *43*, 4212.

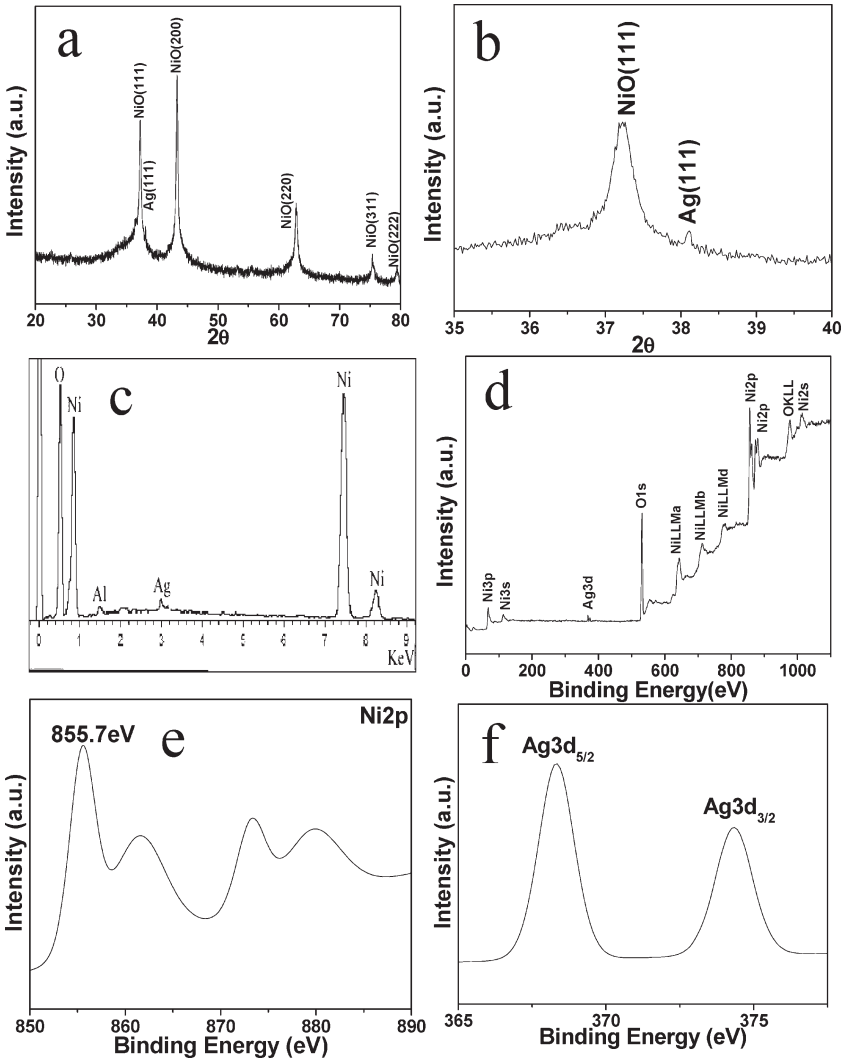

Figure 7. XRD pattern (a, b), EDX pattern (c), and XPS spectra (d−f) of Ag−NiO nanotubes.

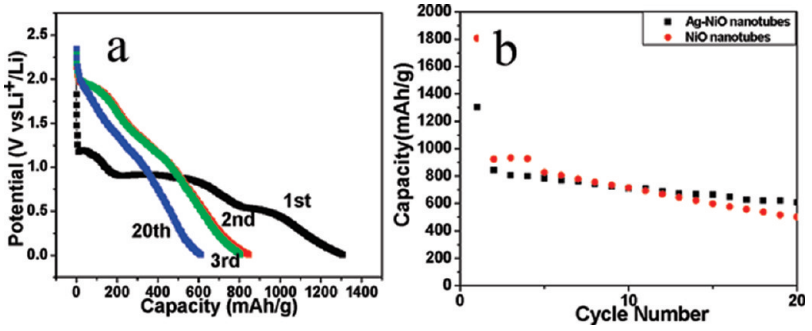

Figure 8. (a) 1st, 2nd, 3rd, and 20th discharge curves of the polycrystalline Ag−NiO nanotube-based anode material at a current density of 100 mA g^{-1} and at room temperature. (b) Discharge capacity versus cycle number for the Ag−NiO nanotubes and pure NiO nanotube-based anode materials at a current density of 100 mA g^{-1} and at room temperature.

exhibit better cycling performance than pure NiO films as negative-electrode.[38] Therefore, the as-synthesized Ag−NiO nanotubes are expected to exhibit the enhanced Li-ion battery performance as the negative-electrode. Figure 8a shows the 1st, 2nd, 3rd, and 20th discharge curves of the Ag−NiO nanotube-based negative-electrode at a current density of 100 mA g^{-1} and room temperature. The discharge curve of the first cycle has two sloping potential ranges, corresponding to the reduction reaction from NiO to Ni (0.5−0.75 V) and the formation of solid electrolyte interface (SEI) film (0.75−1.25 V), respectively. The discharge capacities of the electrode in the 1st, 2nd, 3rd, and 20th cycles are 1305.1, 845, 806.4, and 607.8 mA h g^{-1}. The nanotubular structure, large surface-to-volume ratio, and the formation

(38) Huang, X. H.; Tu, J. P.; Zeng, Z. Y.; Xiang, J. Y.; Zhao, X. B. *J. Electrochem. Soc.* **2008**, *155*, A438.

of SEI film may be responsible for the high capacity in the first cycle. It can be calculated that the initial coulomb efficiency of Ag−NiO nanotube-based negative-electrode is about 65%, which is higher than that of pure NiO nanotubes (51.2%). It is believed that the combining of Ag can enhance the electronic conductivity of the active materials, leading to higher initial coulomb efficiency. After 20 cycles, the capacity of the Ag−NiO nanotube-based negative-electrode is still significantly higher than the theoretical capacity of commercial carbon. Figure 8b shows discharge capacity versus cycle number at a current density of 100 mA g^{-1} at room temperature when Ag−NiO or NiO nanotubes are employed. It is clear that the capacity of the Ag−NiO nanotubes is smaller than that of pure NiO nanotubes in the first cycle because the addition of Ag occupies the effective mass but has no contribution for the capacity. However, the combining of Ag can improve the initial coulomb efficiency and cycle performance due to the enhanced electronic conductivity of the active materials. The capacity of Ag−NiO nanotubes surpasses that of pure NiO nanotubes from the 10th cycle. After 20 cycles, the capacity of the Ag−NiO nanotubes is 607.8 mA h g^{-1}, which is significantly higher than that of pure NiO nanotubes (501.3 mA g^{-1}).

Conclusions

In summary, we have developed an LBL method to synthesize composite metal oxide nanotubes by using CNTs as the template in combination with subsequent calcination. The electrostatic attraction between the charged species plays the most important role in the formation of CNTs-based core−shell nanotubes, which is a prerequisite for the preparation of composite metal oxide nanotubes. This method is representatively demonstrated by the preparation of CeO_2−SnO_2 and Ag−NiO composite nanotubes. The nanotubular structure and compositing of these nanotubes lead to superior performance when CeO_2−SnO_2 and Ag−NiO nanotubes are used in gas sensors and Li-ion batteries, respectively. It is hoped that the method introduced in this work may be extended to synthesize a variety of important composite nanotubes.

Acknowledgment. The authors would like to acknowledge financial support from the 973 Project (No. 2007CB613403), NSFC (No. 50802086), Zijin Project, ZJPNSFC (Y407138), and the Doctoral Program of the Ministry of Education of China (No. 20070335014).